Road Surface Quality Assessment Using Polarimetric Airborne SAR

Arun Babu
Microwaves and Radar Institute
German Aerospace Center (DLR)
Wessling, Germany
arun.babu@dlr.de

Stefan V. Baumgartner
Microwaves and Radar Institute
German Aerospace Center (DLR)
Wessling, Germany
stefan.baumgartner@dlr.de

***Abstract*— Since the road infrastructure is an important factor for the economy and safety, the continuous monitoring of the road condition is a necessity. Compared to the widely used costly, time consuming and labour-intensive road condition monitoring using measurement vehicles all over the country, the potential of SAR polarimetry to remotely monitor the road surface roughness, cracks and potholes are investigated in this study. The polarimetric analysis of fully polarimetric X-band radar datasets acquired over the Kaufbeuren test site with DLR's airborne sensor F-SAR revealed that the anisotropy and coherency matrix (T3) elements are sensitive to the road surface roughness and can be used to retrieve the vertical surface roughness. The cross-polar sigma nought images show a considerable increase in their magnitude over the cracks and potholes on the road surface. The initial experimental results obtained from this study are discussed in this paper.**

Keywords*— *F-SAR, Polarimetry, Sigma nought, Road surface roughness, Anisotropy, Coherency matrix

I. Introduction

The road network has a crucial contribution to the economic and social development of a country. So, it should be considered as the most important of all public assets [1]. The ride quality and safety of the vehicles depends on the quality of the road. The cracks, potholes and surface roughness are the important factors which affect the road surface quality [2]. The potholes occur as a result of the repeated expansion and contraction during freeze-thaw water cycles, combined with the amount of traffic on the pavement. Potholes mostly appear in late winter and early spring due to the changing temperatures. The repeated freezing and thawing of melting snow combined with the spring rain weakens the pavements leading to cracks and potholes[3]. The cracks and potholes cause damage to the tyres, wheels, exhaust system, suspension and even the engine of the vehicles leading to accidents, increased maintenance costs and reduces the lifetime of the vehicles. Also, the road surface roughness is one of the important parameters which directly affect the stability of the vehicles on the roads. Road surface roughness influences the 'grip' or 'skid resistance' of the vehicle. Sufficient amount of skid resistance is required for performing safe acceleration, deceleration and steering manoeuvres. Several studies have proven that poor skid resistance leads to a higher accident probability [4].

Because of all these reasons, the road infrastructure needs to be monitored periodically to keep track of the changes in its condition so that the required maintenance works can be carried out immediately when degradation in the road quality is detected. But, in most of the countries, the road condition is measured only once in several years. One of the main reasons for this is the enormous costs required because the road condition is measured manually by driving measurement vehicles all over the country which is a labour-intensive and time-consuming process [5]. This study focuses on evaluating the potential of polarimetric airborne SAR to remotely estimate the road surface conditions on a large scale. So far, not much literature for road surface roughness estimation is available. The prime objective of this study is to investigate and develop efficient and reliable methods for road surface roughness estimation and also for the detection of cracks and potholes.

II. Mathematical Relationships and Algorithms

A. Road surface roughness estimation

The Polarimetric Synthetic Aperture Radar (PolSAR) is an advanced imaging radar system which uses the different polarization states of an Electromagnetic (EM) wave of the same centre frequency to analyse the scattering information from different ground targets on the Earth's surface [6].

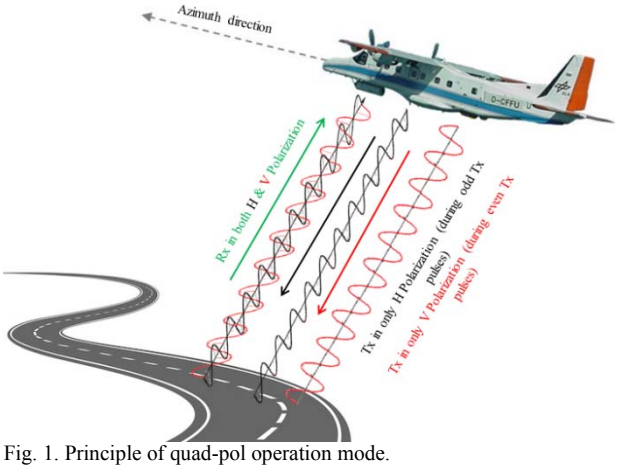

Fig. 1. Principle of quad-pol operation mode.

In a fully polarimetric SAR system in quad-pol operation mode, first, a horizontally polarized EM wave is transmitted (during odd transmission pulses) and both horizontal and vertical polarized EM waves backscattered by the ground targets are received simultaneously (Fig. 1). After receiving all the backscattered EM waves from near range to far range, the vertically polarized EM wave is

978-1-7281-8942-0/20/$31.00 ©2020 European Union

transmitted (during even transmission pulses) and the horizontal and vertical polarized backscattered EM waves are received (Fig. 1). So from a quad-pol SAR system, 4 channels can be obtained: horizontal polarization transmitted and horizontal (S_{HH}) and vertical polarization (S_{HV}) received simultaneously; vertical polarization transmitted and horizontal (S_{VH}) and vertical polarization (S_{VV}) received simultaneously [7]. The polarimetric information obtained as 4 channels can be represented in the form of the Pauli basis vector (k_p) as follows [8]:

$$k_p = \frac{1}{\sqrt{2}}\begin{pmatrix} S_{HH} + S_{VV} \\ S_{HH} - S_{VV} \\ 2S_{HV} \end{pmatrix}. \quad (1)$$

By multiplying the Pauli basis vector with the transpose of its complex conjugate, the 3x3 coherency matrix $T3 = k_p \,.\, k_p^{*T}$ can be obtained as [9], [10]:

$$T3 = \frac{1}{2}\begin{bmatrix} \langle|S_{HH} + S_{VV}|^2\rangle & \langle(S_{HH} + S_{VV})(S_{HH} - S_{VV})^*\rangle & 2\langle(S_{HH} + S_{VV}).S_{HV}\rangle \\ \langle(S_{HH} - S_{VV})(S_{HH} + S_{VV})^*\rangle & \langle|S_{HH} - S_{VV}|^2\rangle & 2\langle(S_{HH} - S_{VV}).S_{HV}{}^*\rangle \\ 2\langle S_{HV}\,.(S_{HH} + S_{VV})^*\rangle & 2\langle S_{HV}\,.(S_{HH} - S_{VV})^*\rangle & 4\langle|S_{HV}|^2\rangle \end{bmatrix}. \quad (2)$$

The coherency matrix $T3$ can be used to derive the polarimetric parameters sensitive to the Root Mean Square (RMS) height (h_{rms}) which is widely used for the vertical roughness characterization [11]:

$$h_{rms} = \sqrt{\frac{\sum_{i=1}^{n}(h_i - \bar{h})^2}{n-1}}. \quad (3)$$

where h_i is the vertical height at location i and $\bar{h}$ represents the mean vertical height of the surface for n samples [11], [12].

From the PolSAR data, the remotely sensed parameter (ks) can be derived which represents the effective vertical roughness. In this study, the polarimetric scattering anisotropy generated from the eigenvalues of the coherency matrix $T3$ and the elements of the $T3$ matrix itself is considered to generate the ks parameter.

According to the eigen-decomposition theorem, the 3x3 coherency matrix $T3$ can be represented as follows [13]:

$$T3 = [U_3][\Sigma_3][U_3]^{-1}. \quad (4)$$

The 3x3 real, diagonal matrix $[\Sigma_3]$ contains the eigenvalues of T3 [14]:

$$[\Sigma_3] = \begin{bmatrix} \lambda_1 & 0 & 0 \\ 0 & \lambda_2 & 0 \\ 0 & 0 & \lambda_3 \end{bmatrix}. \quad (5)$$

where $\infty > \lambda_1 > \lambda_2 > \lambda_3 > 0$.

The anisotropy parameter (A) is generated as follows [9], [14], [15]:

$$A = \frac{\lambda_2 - \lambda_3}{\lambda_2 + \lambda_3}. \quad (6)$$

The effective vertical roughness ks can be estimated from anisotropy as follows [11], [12]:

$$ks = 1 - A. \quad (7)$$

So, the ks estimated using the anisotropy parameter is based on the 2nd and 3rd eigenvalues of the coherency matrix.

The ks can also be estimated from the T_{22} and T_{33} elements of the coherency matrix as follows [9][12]:

$$ks = 1 - \frac{T_{22} - T_{33}}{T_{22} + T_{33}}. \quad (8)$$

The Root Mean Square (RMS) height (h_{rms}) can be derived from the ks using the following equation:

$$h_{rms} = \frac{ks}{(2\pi/\lambda_c)}. \quad (9)$$

where λ_c is the centre frequency of the SAR system.

B. *Cracks and potholes detection*

The radiometrically calibrated sigma nought (σ^0) images of the four polarization channels are analysed to investigate the effects of cracks and potholes in the co-polarized and cross-polarized channels. The sigma nought (σ^0) images are calculated as follows [16]:

$$\sigma_{dB}^0 = 10 \cdot \log_{10}(|I|^2 \sin\theta_{inc}.\ ) \quad (10)$$

where θ_{inc} is the local incidence angle and I is the single-look complex (SLC) image of the respective channel.

III. PRELIMINARY EXPERIMENTAL RESULT

This study was started in September 2019 and the initial results of the road surface roughness, cracks and potholes estimated using the techniques described in the previous section are discussed here.

A. *Experimental data*

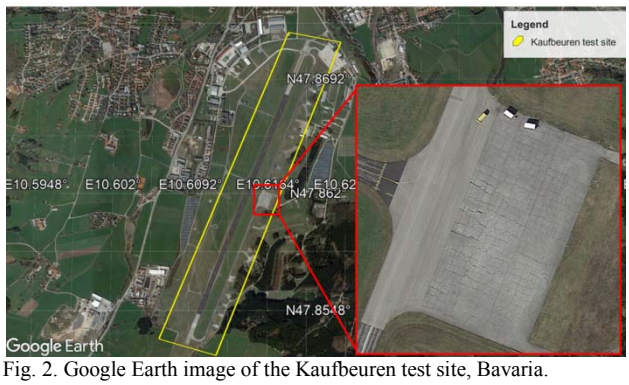

Fig. 2. Google Earth image of the Kaufbeuren test site, Bavaria.

X-band quad-pol data acquired with DLR's airborne F-SAR sensor over the Kaufbeuren test site (Fig. 2) located in Bavaria are used for this study. The test site was a former Military Airfield and includes the runway, taxiways and parking areas composed of different materials (e.g., asphalt, concrete) and, thus, have different surface roughness, also cracks and potholes are present there (see zoomed view inside the red rectangle in Fig. 2).

B. *Road Surface Roughness*

Fig. 3 shows the intensity HH image of the test site. The runway and the cracked parking area are indicated in the image.

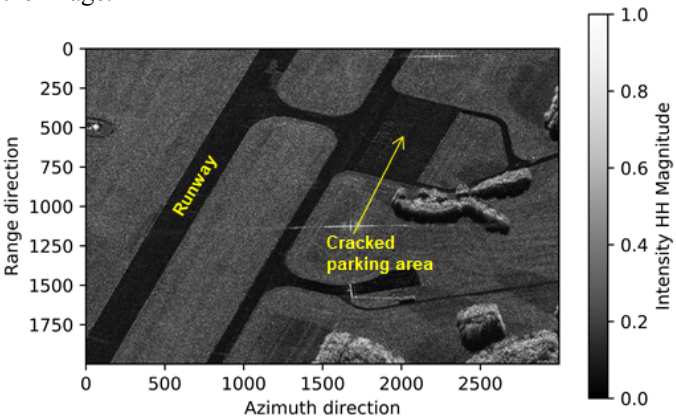

Fig. 3. Intensity HH image of the Kaufbeuren test site

Fig. 4 (a) shows the ks values estimated from the anisotropy parameter. By analysing the image, it can be seen that the roads are having ks values close to zero and the surrounding grasslands are having higher values of ks up to 0.50. But since the anisotropy parameter is estimated from the minor eigenvalues (2nd and 3rd) of the $T3$ matrix, the ks image appears to be noisy.

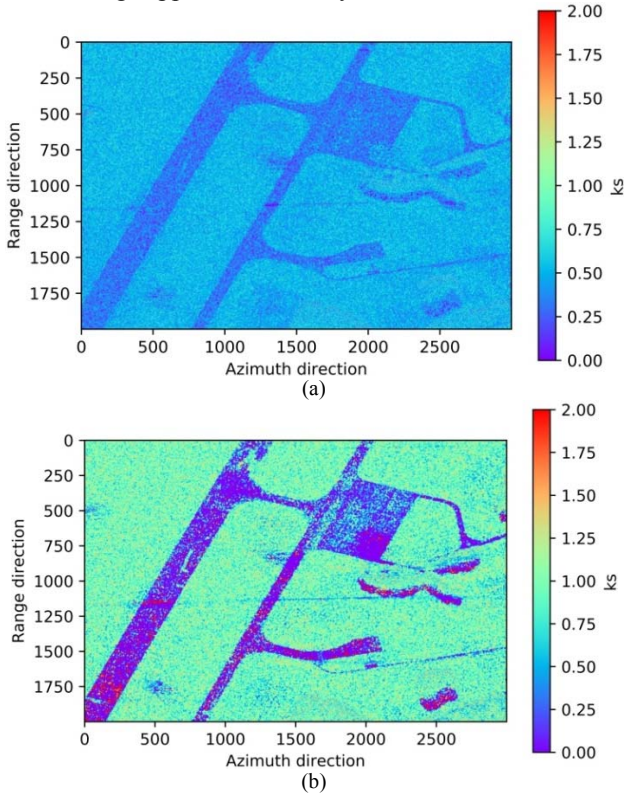

Fig. 4. ks images; (a) obtained from Anisotropy; (b) from T3 matrix.

Fig. 4 (b) shows the ks values estimated from the $T3$ matrix elements. As seen in Fig. 4 (a), in Fig. 4 (b) also the roads are having very low ks in the order of 0, but the surrounding grasslands are having higher values of ks close to 1 which is almost twice as seen in Fig. 4 (a). The ks image generated from $T3$ matrix appears to be less noisy than the ks image generated from Anisotropy parameter (A).

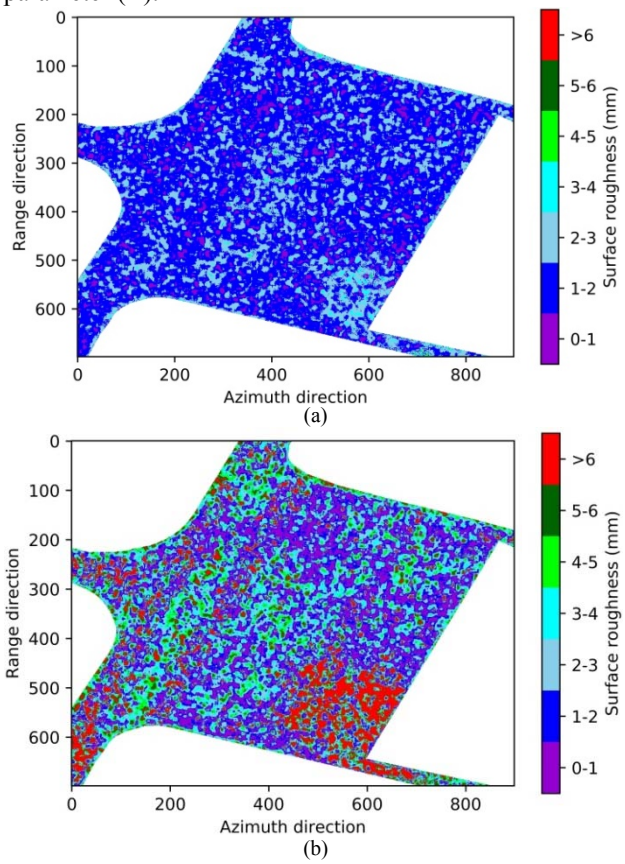

Fig. 5. h_{rms} images of the cracked parking area; (a) from Anisotropy; (b) from T3 matrix.

Fig. 5 (a) shows the h_{rms} image of the cracked parking area shown in Fig. 2 and its surrounding grasslands estimated from the anisotropy parameter. As discussed with the ks image in Fig. 4 (a), the image appears to be noisy. The cracked road areas are showing higher values of h_{rms} and the smooth road sections are showing comparatively lower values of h_{rms} .

Fig. 5 (b) shows the h_{rms} image generated from the $T3$ matrix elements. The similar trend in roughness variation can be observed in both figures. But Fig. 5 (b) shows higher values of roughness for the same areas in Fig. 5 (a).

C. *Cracks and Potholes*

The effect of cracks and potholes on the co-polar and cross-polar sigma nought images are discussed here.

Fig. 6 (a) and (b) shows the co-polar sigma nought images generated from the HH and VV channels respectively. By comparing Fig. 6 (a) with the Google Earth image shown in Fig. 2, it can be seen that even though some of the severe cracks are visible in the sigma nought HH image, the other cracks, potholes and their patterns cannot be identified. The same is valid for the sigma nought VV image (Fig. 6 (b)). However, the sigma nought values may

depend on the aspect angle or direction of the cracks so that by looking to the preliminary results obtained from a single data set no final conclusions regarding the usability of HH and VV can be drawn. So that more analysis is required using datasets acquired with different aspect angles.

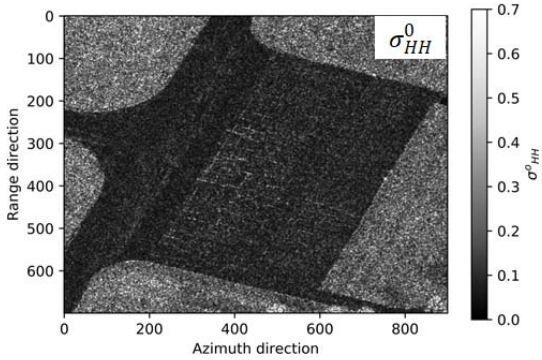

(a)

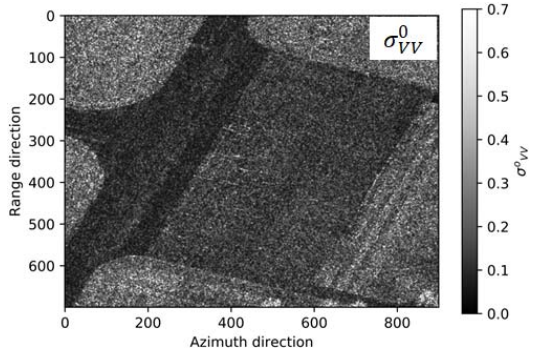

(b)

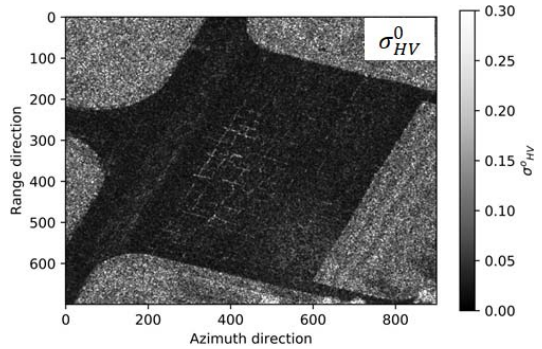

(c)

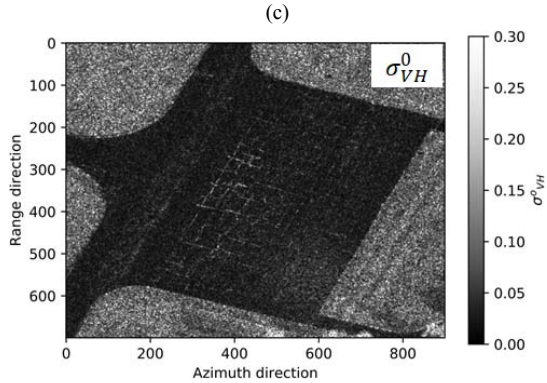

(d)

Fig. 6. Sigma nought (σ^0) images

The cross-polar sigma nought images generated from the HV and VH channels is shown in Fig. 6 (c) and (d) respectively. By comparing both Fig. 6 (c) and (d) with the Google Earth image of the cracked road area (Fig. 2), it can be seen that most of the cracks, potholes and their patterns are clearly visible in the sigma nought HV and VH images.

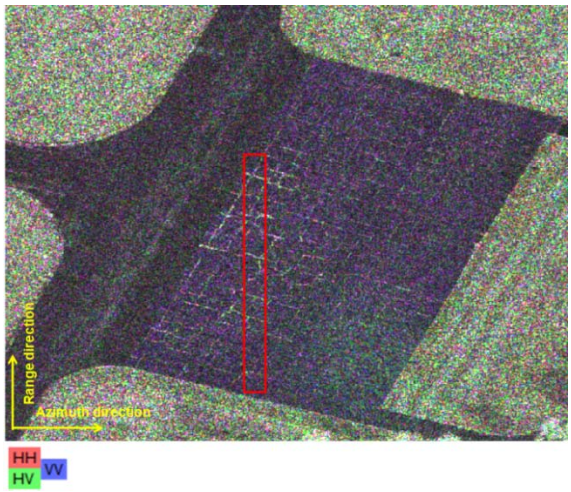

Fig. 7. RGB composite generated from F-SAR intensity images

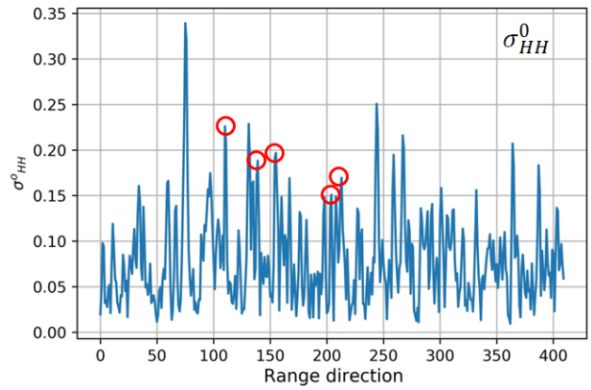

(a)

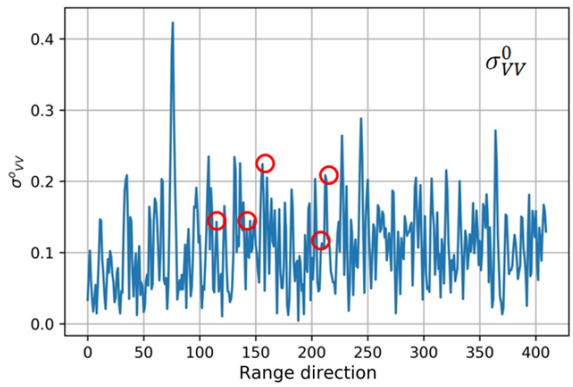

(b)

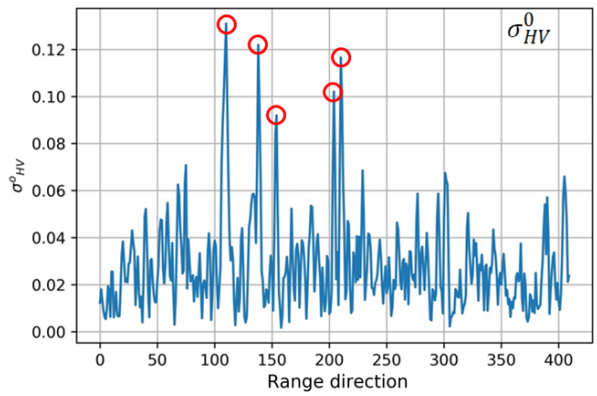

(c)

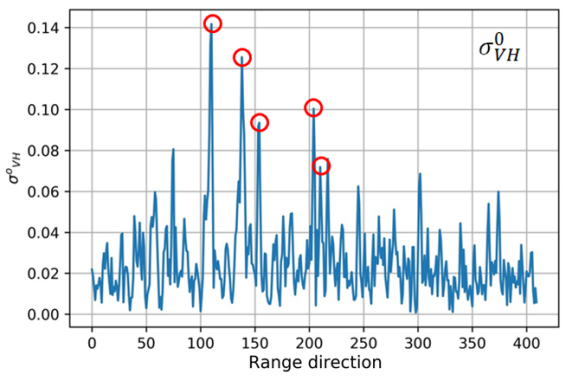

(d)

Fig. 8. Sigma nought (σ^0) magnitude plots.

Fig. 7 shows the RGB composite of the intensity images with HH channel as the red band, HV channel as the green band and VV channel as the blue band. The cracks can be clearly seen in the image and the severely cracked road region inside the red rectangle is chosen to analyse the effect of cracks on co-pol and cross-pol channels.

Fig. 8 (a) and (b) shows the magnitude plots for the co-polar sigma nought HH and VV channels (σ^0_{HH} and σ^0_{VV}), respectively, and the expected crack positions are indicated by the red circles. The plots are generated from the severely cracked road section along the range direction shown inside the red rectangle in Fig. 7. By analysing the sigma nought HH (σ^0_{HH}) magnitude plot it can be seen that there is only a small increase in the order of 0.05 to 0.08 in the cracked road areas compared to the surrounding smooth road sections. The sigma nought VV (σ^0_{VV}) magnitude plot (Fig. 8 (b)) shows that there is a negligible influence of the cracks and potholes on the sigma nought VV (σ^0_{VV}) magnitude.

Fig. 8 (c) and (d) shows the magnitude plots for the cross-polar sigma nought HV and VH (σ^0_{HV} & σ^0_{VH}) channels, respectively. By analysing both the magnitude plots at the cracked positions on the road indicated by red circles, it can be seen that there is a relative increase of magnitude up to approximately 0.13 at the severely cracked road regions compared to the surrounding smooth regions. This means that HV and VH channels are better suited for crack detection than HH and VV channels.

IV. CONCLUSION

Polarimetric data are sensitive to road surface roughness and also to cracks and potholes and thus show great potential for wide-area road surface condition monitoring. The anisotropy and $T3$ matrix elements can be used to retrieve the road surface roughness (h_{rms}). Even in intensity images, larger cracks can be recognized. The cross-polar sigma nought images show a considerable relative increase in their magnitudes compared to the co-polar sigma nought images. The next step is to compare the results to the ground truth data. A sensitivity analysis has to be carried out, especially w.r.t. the influence of SNR on the estimated road surface roughness h_{rms}. The $T4$ matrix based noise mitigation method can be used to minimize the additive noise present in the polarimetric data and for SNR estimation. Additionally, SAR backscatter based models can be used for the road surface roughness estimation. These investigations are currently in progress. Further experiments are planned using a Ka-band sensor which, due to the smaller wavelength, will be much more sensitive to the roughness differences and suitable for detecting smaller cracks and potholes.

REFERENCES

[1] G. Malkoc, "The importance of road maintenance," *World Highways* , 15-Jul-2015. [Online]. Available: https://www.worldhighways.com/wh8/wh9/wh10/feature/importance-road-maintenance. [Accessed: 06-Jul-2020].

[2] S. Sattar, S. Li, and M. Chapman, "Road surface monitoring using smartphone sensors: A review," *Sensors*, vol. 18, no. 11, 2018.

[3] S. Biswas, "Pothole Condition in Canada and Evaluation of Maintenance Material," University of Alberta, 2016.

[4] H. Liu, Z. Zhang, D. Guo, L. Peng, Z. Bao, and W. Han, "Research progress on characteristic technique of pavement micro-texture and testing technology of pavement skid resistance at home and abroad," in *2011 International Conference on Remote Sensing, Environment and Transportation Engineering*, 2011, pp. 4368–4372.

[5] K. Laubis, "Crowd-Based Road Surface Monitoring and its Implications on Road Users and Road Authorities," Karlsruhe Institute of Technology, Germany, 2017.

[6] C. Si-wei, X. Wang, S.-P. Xiao, and Sato M, *Target Scattering Mechanism in Polarimetric Synthetic Aperture Radar Interpretation and Application*. Singapore: Springer Nature, 2018.

[7] C. E. Livingstone, I. Sikaneta, C. Gierull, S. Chiu, and P. Beaulne, "RADARSAT-2 System and Mode Description," Ottawa, 2015.

[8] I. H. Woodhouse, *Introduction to microwave remote sensing*. New Delhi, India: CRC Press, Taylor & Fancis Group, 2009.

[9] I. Hajnsek, "Inversion of Surface Parameters Using Polarimetric SAR," Friedrich Schiller University Jena, 2001.

[10] J. Van Zyl and Y. Kim, *Synthetic Aperture Radar Polarimetry*, 1st editio. New Jersey: Wiley-Blackwell, 2011.

[11] P. Marzahn and R. Ludwig, "On the derivation of soil surface roughness from multi parametric PolSAR data and its potential for hydrological modeling," *Hydrol. Earth Syst. Sci.*, pp. 381–394, 2009.

[12] T. Jagdhuber, "Soil Parameter Retrieval under Vegetation Cover Using SAR Polarimetry," University of Potsdam, 2012.

[13] C. M. H. Unal and L. P. Ligthart, "Decomposition Theorems applied to Random and Stationary Radar Targets," *Prog. Electromagn. Res.*, pp. 45–66, 1998.

[14] E. Pottier, J.-S. Lee, and L. Ferro-Famil, "Advanced Concepts in Polarimetry – Part 1," vol. 2, no. October, pp. 21–22, 2004.

[15] J. A. Richards, *Remote Sensing with Imaging Radar*. Springer International Publishing, 2009.

[16] M. Keller, J. Fischer, and M. Jager, "F-SAR Product Description," Microwaves and Radar Institute, German Aerospace Center (DLR), Oberpfaffenhofen, 2016.